Exp Fluids (2015) 56:201
DOI 10.1007/s00348-015-2077-5

RESEARCH ARTICLE

Passive jet control of flow around a circular cylinder

Wen-Li Chen[1,2,3] · Dong-Lai Gao[1,2] · Wen-Yong Yuan[1,2] · Hui Li[1,2] · Hui Hu[3]

Received: 18 July 2015 / Revised: 14 September 2015 / Accepted: 23 October 2015 / Published online: 30 October 2015

Abstract In the present study, a passive flow control method, which is featured by passive windward suction combined with leeward jet over a circular cylinder for drag reduction and dynamic wind loading suppression, was experimentally investigated to manipulate unsteady wake vortex shedding from a circular cylinder. Four perforated pipe designs with different numbers of suction/jet holes (i.e., from 2 to 24 suction/jet holes) were used to create flow communicating channels between the windward and leeward stagnation points of a cylindrical test model. The experimental study was performed in a wind tunnel at a Reynolds number of $Re = 4.16 \times 10^4$ based on the cylinder diameter and oncoming airflow speed. In addition to measuring surface pressure distributions to determine the dynamic wind loads acting on the test model, a digital particle image velocimetry (PIV) system was also used to quantify the wake flow characteristics in order to assess the effectiveness of the passive jet control method with different perforated pipe designs, in comparison with a baseline case without passive jet control. It was found that the passive jet control method is very effective in manipulating the wake vortex shedding process from the circular cylinder. The perforated pipe designs with more suction/jet holes were found to be more effective in reducing drag and suppressing fluctuating amplitude of the dynamic wind loads acting on the test model. With 24 suction/jet holes evenly distributed over the cylindrical test model (i.e., the N13 design of the present study), the passive jet control method was found to be able to achieve up to 33.7 % in drag reduction and 90.6 % in fluctuating wind loading suppression, in comparison with the baseline case. The PIV measurement results revealed clearly that the passive jet control method would cause airflow jets into the cylinder wake and change the shedding modes of the wake vortex structures from the cylindrical test model. Because of the dynamic interactions between the passive jets and the wake vortex structures, the antisymmetric pattern of the wake vortex shedding was found to be converted to symmetric mode. The periodicity of the vortex shedding was also observed to be diminished and eventually disappeared with the number increase in the suction/jet holes. A linear stability analysis was performed to suggest that the passive jet flow would modify the wake stability of the circular cylinder by decreasing the disturbance growth rate in the immediate wake and pushing the region of absolute instability further downstream.

1 Introduction

Long and flexible cable structures are commonly used in bridge engineering, such as stay cables of cable-stayed bridges, vertical hangers of suspension bridges. Because of relatively low stiffness and damping ratios, cable structures are susceptible to wind and may suffer from oscillatory instabilities. For example, vortex-induced vibration (VIV) and rain-wind-induced vibration (RWIV) of stay cables have been reported in previous studies (Zuo and Jones 2010; Hikami and Shiraishi 1988). When exposed to

✉ Wen-Li Chen
cwl_80@hit.edu.cn

[1] Key Lab of Structures Dynamic Behavior and Control (Harbin Institute of Technology), Ministry of Education, Harbin 150090, Heilongjiang, China

[2] School of Civil Engineering, Harbin Institute of Technology, Harbin 150090, Heilongjiang, China

[3] Department of Aerospace Engineering, Iowa State University, Ames 50011, IA, USA

wind, as any bluff body, cables with a circular cross section are characterized by flow separation and vortex shedding downstream in the near wake. Vortices are originated from the rollup of the unstable shear layers generated at the separation point, and the alternating vortex shedding can induce large unsteady side force acting on the cylinder (Brika and Laneville 1993). As the shedding frequency approaches some order of the natural frequency of a given oscillating cylinder, a resonant response tends to develop freely. As a result, the vortex shedding frequency may be captured by the natural frequency of the cylinder, this fluid–structure synchronization often referred to as 'lock-in', may induce significant vibrations of the cables.

Extensive studies have been conducted in recent years to explore various techniques for effective suppression of vortex-induced vibrations of circular cylinders. A number of passive control methods have been proposed to reduce the drag, suppress the fluctuating lift, and manipulate the wake vortex shedding from circular cylinders, including surface protrusions, splitter plates, guiding vanes, base-bleed (Zdravkovich 1981). Owen and Bearman (2001) attached hemispherical bumps to force the separation lines of circular cylinders to be sinuous, up to 47 % drag reduction was achieved by using the passive flow control method.

Active flow control methods based on flow suction or blowing have also been suggested to suppress vortex-induced vibration of circular cylinders. Amitay et al. (1997) introduced fluidic actuators based on synthetic jet technology to modify the aerodynamic shape and control the boundary layer flow separation over a circular cylinder. Their experiment demonstrated that because of the interaction of the jets with the boundary layer flow, closed recirculating flow regimes were formed near the rear end of the cylinder surface. They indicated that the closed recirculating flow regimes could act as a "virtual surface" to displace local streamlines outside, as a result, reduced drag up to 30 %. Since then, a number of studies were conducted to confirm that synthetic jet is an effective way to control flow separation over a circular cylinder, which can diminish or even completely eliminate the flow separation (Amitay et al. 1998; Crook et al. 1999; Fujisawa and Takeda 2003; Glezer et al. 2003; Wolfe and Ziada 2003; Fujisawa et al. 2004). As a result, drag was reduced and the development of resonant response was also suppressed. Feng et al. (2010, 2011) and Feng and Wang (2010, 2012) conducted a series of experimental studies and found that synthetic jets located at the rear stagnation points of circular cylinders could be used to impose symmetric perturbations on the cylinder flows and result in a modification of the vortex shedding mode. Chen et al. (2013) used a steady-suction-based active flow control method to suppress the wake vortex shedding, thereby the vortex-induced vibration of a circular cylinder. Their experimental results indicated that the steady-suction-based flow control method exhibits excellent control effectiveness and can distinctly suppress the vortex-induced vibration by dramatically reducing the amplitudes of cylinder vibrations, fluctuating pressure coefficients and lift coefficients of the circular cylinder.

Dong et al. (2008) conducted a numerical study to demonstrate that a flow control method with windward suction and leeward blowing (WSLB) would be more effective than suction-only/blowing-only in lift suppression. A stability analysis was also performed to reveal that the region of absolute instability shrunk and was displaced further downstream with WSLB control in the near wake, which gave a thorough understanding of the underlying mechanism of the WSLB control. It should be noted that the WSLB method suggested by Dong et al. (2008) is an active flow control method in the sense that external energy is needed to maintain the suction and blowing. While active flow methods are usually more effective and convenient to operate for optimized flow control effectiveness, in comparison with passive flow control methods, almost all the active flow control schemes are costly from the implementation standpoint since they require excessive energy expenditures to maintain the optimized flow control effectiveness. While WSLB method proposed by Dong et al. (2008) is an active flow control method, it can be easily implemented as a passive flow control scheme by adopting porous surfaces or forming communicating channels between the windward and leeward stagnation points of circular cylinders. Following up the work described in Dong et al. (2008), Baek and Karniadakis (2009) successively investigated flow around a geometrically modified circular cylinder with a slit parallel to the incoming flow. The slit was used to form a communicating channel between the windward and leeward stagnation points. The numerical simulation results of Baek and Karniadakis (2009) suggested that the existence of slit was effective in suppressing vortex-induced vibration by changing the vortex shedding mode. The slit with sufficiently large width could cause strong airflow jets into the wake and interact with the wake vortices behind the cylinder. Furthermore, when the slit was larger than the critical width, the instantaneous wake vortex shedding did not show any periodicity. Despite its distinctive flow control effectiveness, it would be quite difficult to adopt for various engineering applications because the slit configuration suggested by Baek and Karniadakis (2009) would impair the structure integrity of the circular cylinder and cause nonlinear instability of the long and flexible cables. Perforated thin shells covering on circular cylinders can be an alternative design for practical implementations.

In the present paper, we aim to develop a passive flow control method for cable structures with circular cross sections. Inspired by the previous studies of Dong et al. (2008) and Baek and Karniadakis (2009), a passive jet flow control

method, characterized by passive windward suction combined with leeward jet, is introduced and experimentally investigated in order to manipulate unsteady wake vortex shedding from a circular cylinder for drag reduction and suppression of dynamic wind loadings acting on a cylindrical test model. In the context that follows, while the configurations of the cylindrical test model to implement the passive jet control and experimental details are introduced in Sect. 2, surface pressure and PIV measurement results are presented and discussed in Sect. 3, followed by some conclusions and discussions in Sect. 4.

2 Configuration and experimental details

2.1 Test model with passive jet control

The experimental study was conducted in a wind tunnel affiliated to the Joint Laboratory of Wind Tunnel and Wave Flume, Harbin Institute of Technology, P. R. China. This closed-circuit wind tunnel has a test section of 505 × 505 mm^2, and the walls of the test section are optically transparent. With honeycombs and mesh structures mounted upstream, a contraction section is installed ahead of the test section to produce uniform incoming flow to enter the test section. The turbulence intensity level in the test section of the wind tunnel was found to be about 0.36 %, measured by using a hotwire anemometer.

Figure 1 shows the schematic of the cylindrical test model used in the present study. The cylindrical model, with the diameter of 70 mm and the spanwise length of 505 mm, was mounted horizontally into the test section of the wind tunnel. The test model was firmly mounted without any detectable free vibration or flow-induced vibration during the experiments. Fifteen passive jet pipe units with the length of 30 mm, which were made of hard plastic and manufactured by using a 3D printer, were symmetrically arranged along the spanwise direction of the cylindrical model. With the thickness of 4 mm and an outer diameter of 78 mm, two pressure measurement planes, which were also made with 3D printer technology, were arranged between the pipe unit in the mid-span and its two neighbors.

To provide a reference to evaluate the effectiveness of the proposed passive jet control technique, a baseline case without any flow control was also performed in the present study. Note the diameter of the uncontrolled cylinder used in the baseline case was 78 mm, consistent with the outer diameter of the modified cylinders. The speed of the incoming airflow was fixed at 8.0 m/s for all the test cases. The corresponding Reynolds number, based on the diameter of the test model and the incoming flow velocity, is $Re = 4.16 \times 10^4$, which is a typical level of Reynolds number for wind-induced vibration of stay cables, as reported in Zuo et al. (2008).

2.2 Passive jet flow control configuration

To form a flow communicating channel between the windward and leeward stagnation points of the circular cylinder, we developed some passive jet flow control pipe units (as shown in Figs. 2, 3). The inner diameter of the pipe unit is 70 mm, which is the diameter of the cylindrical test model. With an overall thickness of 4 mm and a length of 30 mm, the pipe units are made with high-resolution 3D printer technology. Since the thickness of the shells has been set as 1.0 mm, the size of the hollow flow channel is 28 × 2 mm^2. Figure 3 illustrates the schematic of a passive jet flow control pipe unit with 5 suction holes on the windward surface and 5 jet holes on the leeward surface. Suction and jet holes are symmetrically arranged on the windward and leeward sides of the circular cylinder. The geometry shape of the suction/

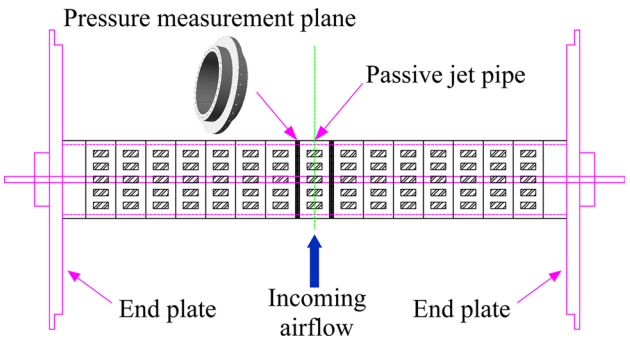

Fig. 1 Top view of the cylindrical test model

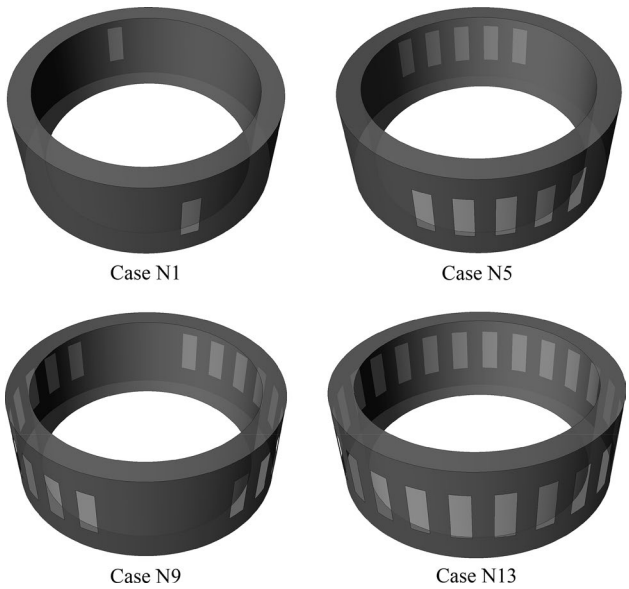

Fig. 2 Schematic drawing of the passive jet control pipe units

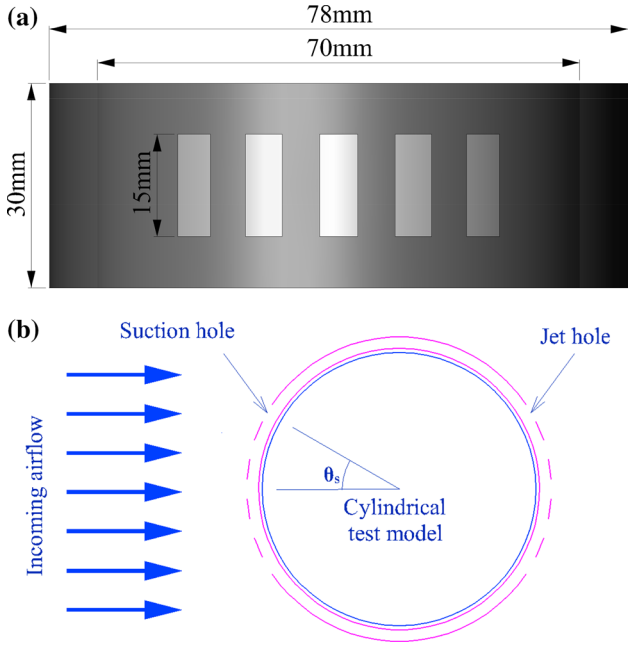

Fig. 3 Schematic of the passive jet control technique with 5 suction holes (i.e., test case N5). **a** Front elevation. **b** Cutaway view

jet holes is rectangular, and the length of each hole is 15 mm, i.e., half of the length of each pipe unit, as shown in Fig. 3a. The interval angle between two neighboring holes equals 15°, and the width in circumferential direction of the suction/jet holes accounts for 7.5° (see Fig. 3b). It should be noted that the only difference of these control pipe units lies in the number of the symmetrically arranged suction/jet holes. The control process of the passive jet technique proposed here can be described as follows: when a circular cylinder with passive jet pipe units is exposed to wind, the incoming airflow would blow into the suction holes on the windward surface of the pipe units. After passing through the communicating channel, the airflow would be exhausted as high-speed jets into the near wake of the circular cylinder through the jet holes. This control scheme is passive in the sense that no external energy input is needed to maintain the flow control.

In the present study, we define a non-dimensional equivalent suction coefficient C_{suc} to characterize the suction capability of different passive jet pipe designs:

$$C_{\text{suc}} = \frac{S_{\text{suc}}}{DH} = \frac{\sum_{i=1}^{N} 0.5H \times \frac{7.5}{360} \times \pi \times D \times \cos\theta_S}{DH} = \sum_{i=1}^{N} 0.5 \times \frac{7.5}{360} \times \pi \times \cos\theta_S = \sum_{i=1}^{N} 0.0104\pi \times \cos\theta_S \quad (1)$$

in which, S_{suc} is the area projection of each suction hole on the plane perpendicular to the incoming flow, D is the diameter of the circular cylinder, H is the length of each pipe, θ_S is the deviation angle between the center line of each suction hole and the incoming flow, and N is the number of suction holes. In the present study, N varies from 1 to 13 with the increment of 4, i.e., 4 controlled cases are experimentally investigated. Based on the number of suction/jet holes arranged on the windward/leeward surface of the pipe, the controlled cases are abbreviated as the test case of N1, N5, N9 and N13, respectively. By the definition given in Eq. (1), C_{suc} values for the 4 test case are 0.0327, 0.1524, 0.2313 and 0.2483, respectively. It can be seen that the value of C_{suc} increases monotonically as the number of the suction holes increases. It is worth noting that for the test case N13, there are 24 suction/jet holes being evenly distributed around the circular cylinder model.

2.3 Experimental setup for surface pressure distribution measurements

A digital pressure measurement system (model DSM3400; Scanivalve Corporation, Liberty Lake, Washington) was used to measure the surface pressure distributions on the cylindrical test model. Seventy-two pressure taps were evenly distributed on two pressure measurement planes, i.e., 36 pressure taps for each. During the experiments, the data acquisition time for instantaneous surface pressure measurements was set to be 30 s with the sampling rate of 625 Hz for all the test cases. In the present study, all the pressure taps were connected by using polyvinyl chloride (PVC) tubes with 0.50 m length and 0.9 mm internal diameter to the pressure transducers. Based on the work described in Irwin et al. (1979), the effect of the tubing system such as the amplitude attenuation and phase lag of the instantaneous pressure signals caused by the 0.9-mm-diameter and 0.5-m-long PVC tubing used for the surface pressure measurements was expected to be quite small and negligible for the present study. The solid blockage and the wake blockage effects of the test model on the pressure measurements were corrected, as suggested by Barlow et al. (1999). In addition, pressure distributions around the two measurement planes were found quite similar due to the symmetry nature of the flow field and the model setup. Therefore, we only present and discuss the pressure results obtained in one measurement plane in the following sections.

After the integration process of the measured surface pressure distributions around the cylinder, the resultant wind loads (i.e., the lift and drag forces) acting on the cylindrical test model could be estimated. The coefficients of the drag and lift forces acting on the cylinder, C_D and C_L are calculated as in Chen et al. (2014):

$$C_D = \frac{1}{2}\sum_i C_{p_i} \cdot \Delta\theta_i \cdot \cos\theta_i\,,$$

$$C_L = \frac{1}{2}\sum_i C_{p_i} \cdot \Delta\theta_i \cdot \sin\theta_i\,,$$

$$C_{p_i} = \frac{p_i - p_\infty}{\frac{1}{2}\rho U_0^2}, \qquad (2)$$

where C_{p_i} is the surface pressure coefficient on the cylindrical test model, p_i is the static pressure on the cylindrical test model, p_∞ is the static pressure of the incoming flow, time series of p_i and p_∞ are obtained and recorded by the digital pressure measurement system. θ_i is the azimuthal angle of the pressure tap, and $\Delta\theta$ is the angle difference between the two neighboring pressure taps, for the present study, $\Delta\theta = 10°$.

It should be noted that the surface pressure measurements were conducted only in the plane between the passive jets for the present study, the surface pressure distributions around the cylindrical test model may vary if the pressure taps are located in other cross-planes on the perforated pipes with the suction/jet holes. Therefore, the estimated aerodynamic forces acting on the test model are expected to be different if the pressure measurement plane is located in other cross-planes on the perforated pipes. It is worth noting that, since the pressure taps used in the present study are actually located in the plane with the greatest distance from the center of the suction/jet holes, the passive jet flow control technique is expected to have least effectiveness in the pressure measurement plane due to the longest distance away from the suction/jet holes. As a result, the flow control effectiveness evaluation based on the surface pressure measurement results would be on the conservative side, which is actually an underestimated estimation on the effectiveness of the passive-jet-based flow control technique in reducing drag and suppressing fluctuating amplitude of the dynamic wind loads acting on the test model.

2.4 Experimental setup for PIV measurements

To quantify the wake flow characteristics behind the cylindrical test model with and without passive-jet-based flow control, a high-resolution particle image velocimetry (PIV) system was employed to conduct detailed flow field measurements in the vertical planes located in the mid-span of the test model. Figure 4 shows the schematic of the experimental setup for the PIV measurements. The incoming airflow was seeded with 1–5 μm oil droplets by using a seeding generator. The vertical plane was illuminated by a double-pulsed Nd:YAG laser adjusted on the second harmonic and emitting two pulses of 200 mJ at the wavelength of 532 nm with a repetition rate of 4 Hz. Manipulated by a set of optics and mirrors, the laser beam was shaped to a thin sheet with a thickness of about 1.0 mm in the target plane. A high-resolution 16-bit CCD camera (PCO 1600, CookeCorp) was used for image acquisition with the axis of the camera perpendicular to the laser sheet. The CCD camera and double-pulsed Nd:YAG lasers were connected to a workstation (host computer) via a Digital Delay Generator (Berkeley Nucleonics, Model 575), which controlled the timing of the laser illumination and the image acquisition.

After acquiring the PIV images, instantaneous velocity vectors were obtained by using frame to frame cross-correlation technique involving successive frames of the patterns of particle images in an interrogation window of 32 × 32 pixels. An effective overlap of 50 % of the interrogation windows was employed in PIV image processing. After the instantaneous velocity vectors (u, v) were determined, instantaneous spanwise vorticity (ω_z) could be derived. The distributions of ensemble-averaged flow quantities, such as the mean velocity ($\overline{U}$,$\overline{V}$), normalized Reynolds stress ($\bar{\tau} = -\overline{u'v'}/U_\infty^2$) and in-plane turbulence kinetic energy (TKE $= 0.5 \times (\overline{u'^2} + \overline{v'^2})/U_\infty^2$), could also be obtained from instantaneous PIV measurements. More than 300

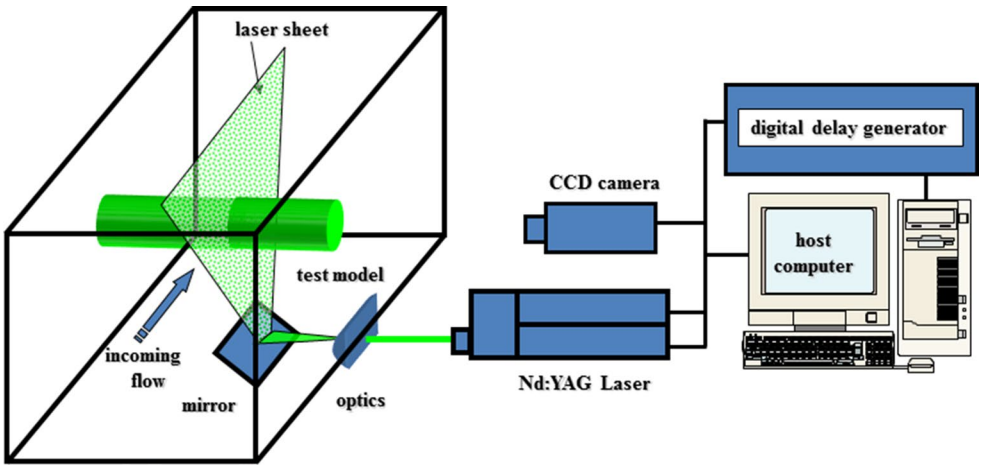

Fig. 4 Schematic of the experimental setup for PIV measurements

frames of instantaneous PIV image pairs were obtained for each case in order to ensure a good convergence of the PIV measurements. For the PIV measurement conducted in the present study, the measurement uncertainty level for the velocity vectors was estimated to be within 2.0 %, while the uncertainties for the measurements of ensemble-averaged flow quantities such as Reynolds stress and turbulent kinetic energy distributions about 5 %.

3 Results and discussions

3.1 Pressure measurement results

Figure 5 gives the measured azimuthal distributions of the pressure coefficients on the surface of the cylinder model for the baseline case and the controlled cases. As expected, Fig. 5a shows a typical pressure distribution around a circular cylinder for the baseline case, i.e., the test case without control. Before the flow separation, the surface pressure on the windward face of the cylinder would recover gradually at $\theta \approx 0°$–$70°$. As the recovery develops, the surface pressure goes into a region characterized with negative pressure gradients on the test model (i.e., $\theta \approx 70°$–$90°$). After that, a large plateau region with a constant low surface pressure coefficient value is found to exist at the leeward side of the test model in the region of $\theta \approx 90°$–$270°$. As revealed by the PIV measurement results to be presented in Sect. 3.2, a large recirculation region is formed in the wake behind the cylinder due to the flow separation. The pressure difference between the windward and leeward face of the cylinder, which is originated from fluid viscosity, results in a drag force acting on the circular cylinder model. Therefore, a general philosophy adopted in drag reduction is to decrease the pressure difference by means of lifting the plateau region in the leeward side of the cylinder. As shown clearly in Fig. 5a, the plateau regions in the leeward side of the cylinder are lifted substantially for all the test cases with passive jet control. Besides, the lifting is also found to be gradually strengthened as the suction capability of the passive jets increases (i.e., characterized by greater C_{suc} value). Moreover, it should be noted that, for the test cases of N9 and N13, the point of flow separation is found to be shifted to $\theta \approx 110°$, indicating a greater drag reduction of the test cases. The mean pressure distributions on the windward side are also found to vary noticeably for the different test cases. Due to the suction effect on the windward side, the windward surface pressure on the circular cylinder is observed to experience a marginal but steady rise, as the value of C_{suc} increases. As shown in Fig. 5b, the root-mean-square (RMS) values of the instantaneous pressure coefficients are also calculated in the present study to quantify the fluctuation amplitudes of the surface pressure distributions around the circular cylinder, which can be used to evaluate the unsteadiness of the dynamic wind loads acting on the cylinder. It can be seen clearly that the RMS values of the instantaneous pressure coefficients on the test model, especially on the leeward side of the cylinder, for the controlled cases are much smaller than that of the baseline case, which indicates a substantial suppression of the unsteady dynamic wind loads acting on the cylindrical model. In general, the measurement results given in Fig. 5 demonstrate that a higher C_{suc} value would contribute to a better effectiveness of the flow control both in drag reduction and unsteady loading suppression.

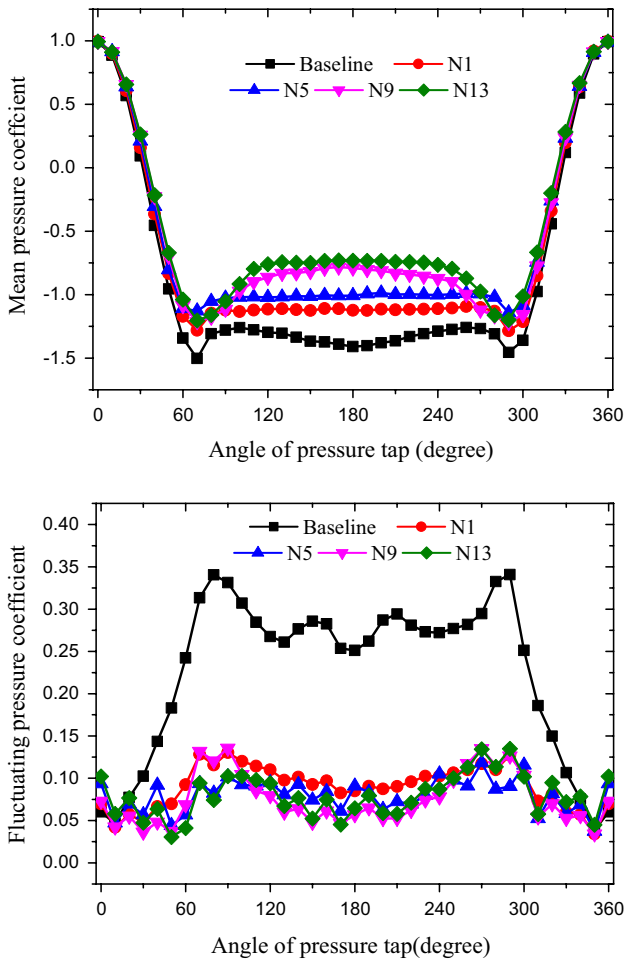

Fig. 5 Mean and fluctuating pressure distributions around the test model with and without passive jet control

The time histories of drag and lift force coefficients of the test model are plotted in Figs. 6 and 7. In the plots, the red dashed lines denote the baseline case, while the black lines represent the controlled cases with different C_{suc} values. Dramatic changes of the drag and lift are observed as the C_{suc} value increases. It can be seen that, for the baseline case, both lift and drag forces acting on the cylinder are highly unsteady with their magnitudes fluctuating

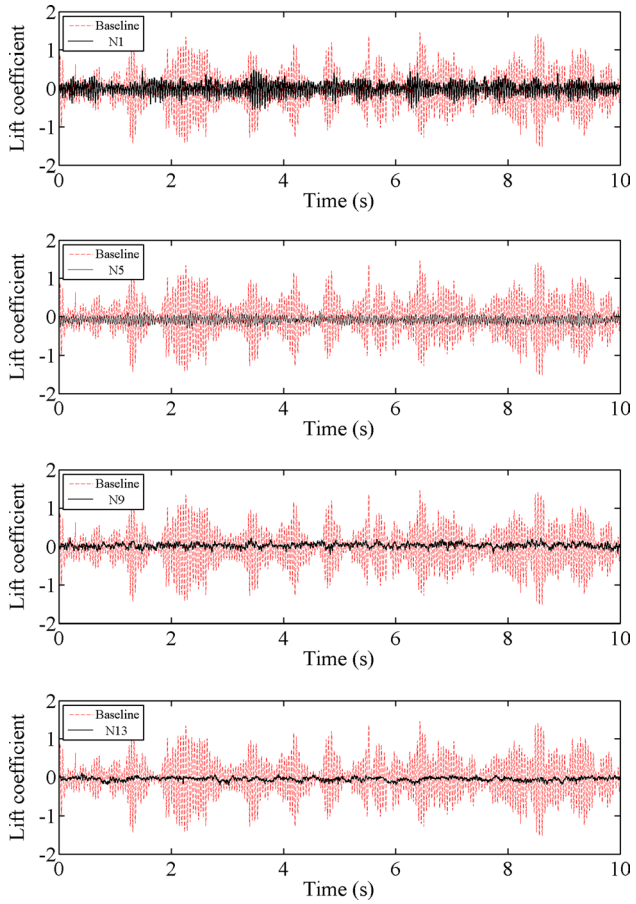

Fig. 6 Time histories of the instantaneous lift coefficients with and without passive jet control

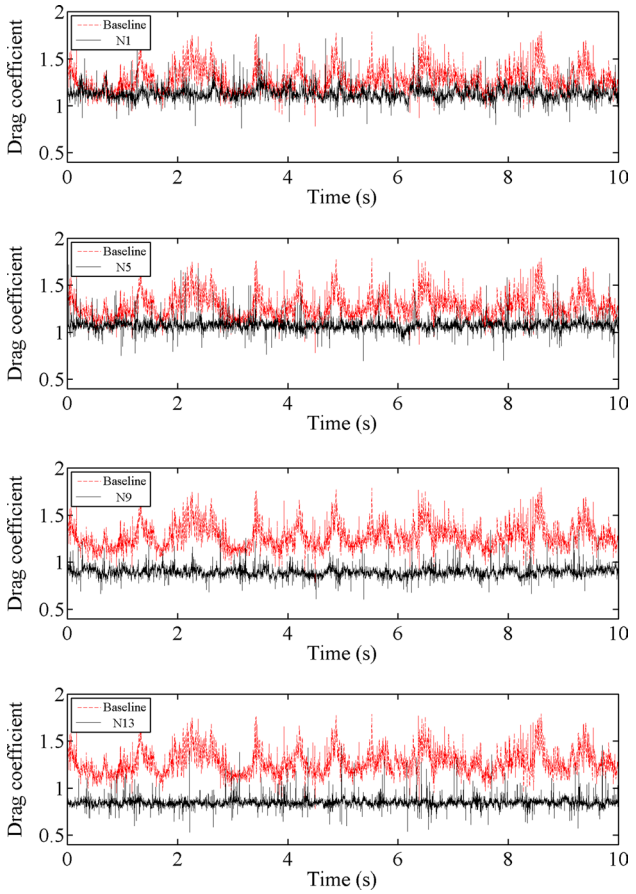

Fig. 7 Time histories of the instantaneous drag coefficients with and without passive jet control

significantly and randomly. This is believed to be closely related to the unsteady vortex shedding in the near wake of the cylinder. As shown in the figures, for the test cases with passive jet control, the fluctuation amplitudes of the instantaneous lift forces acting on the cylinder are considerably suppressed. The unsteady aerodynamic forces acting on the test model are widely considered to be responsible for the excitation of the vortex-induced vibration; hence, the cylinder will be exempted from the vortex-induced vibration with the implementation of passive jet control. Moreover, the mean drag force coefficients of the controlled cases are also found much smaller in comparison with that of the baseline case. It is noticeable that when the value of C_{suc} reaches 0.2313 (i.e., test case N9), the mean drag coefficient is found to be basically below 1.0.

Figure 8 shows the power spectrum of the measured dynamic lift forces acting on the test model through a fast Fourier transform (FFT) analysis. As shown clearly in the plots, the baseline case has a dominant frequency of 21.84 Hz and the corresponding Strouhal number (St) is about 0.21, which is consistent with the measurement data reported in Kondo (1993) and Fransson et al. (2004) for the wake vortex shedding frequency from circular cylinders at the Reynolds number level of the present study. A dominant frequency can also be identified in the power spectrum for the test case N1, indicating a periodicity of the vortex shedding from the circular cylinder. However, the frequency for the test case N1 exhibits a minimal offset from that of the baseline case, which demonstrates that the wake vortex shedding process is indeed influenced by the passive jet control. Moreover, the dominant frequency in the power spectrum is found to diminish or even disappear for all the other test case with more suction/jet holes (i.e., higher C_{suc} values), revealing a gradually enhanced capacity of the passive jet flow control to manipulate the periodic wake vortex shedding process. The experimental observations based on the spectrum analysis are confirmed clearly and quantitatively by the PIV measurement results to be presented in Sect. 3.2.

Based on the time sequences of the measured dynamic aerodynamic forces acting on the cylinder, the time-averaged drag force (i.e., mean drag) and root-mean-squire (RMS) values of the instantaneous lift coefficients for

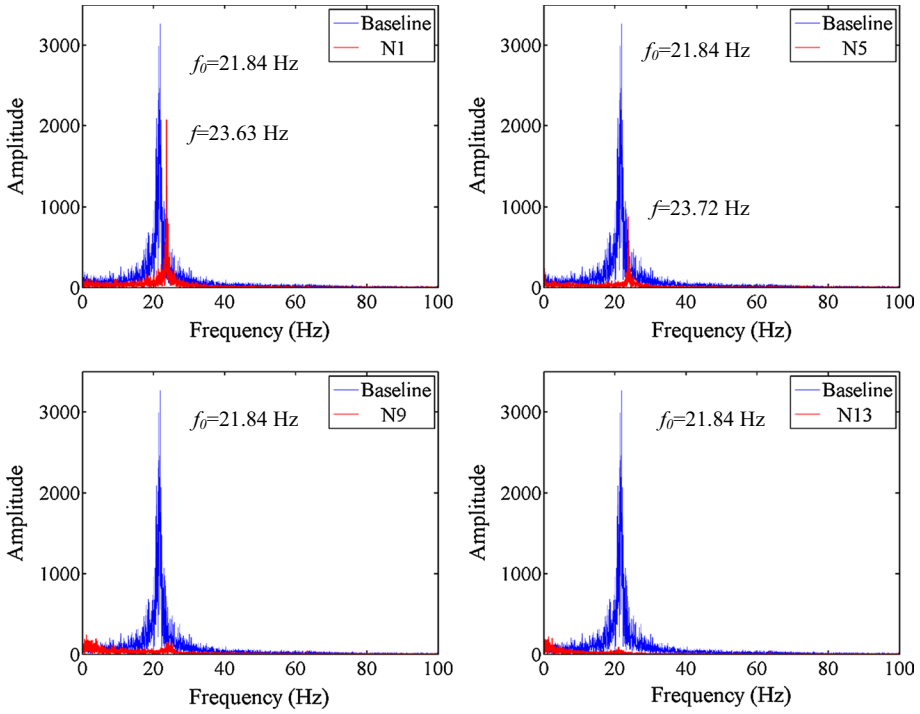

Fig. 8 Power spectrum of the lift forces for different controlled cases versus the baseline case

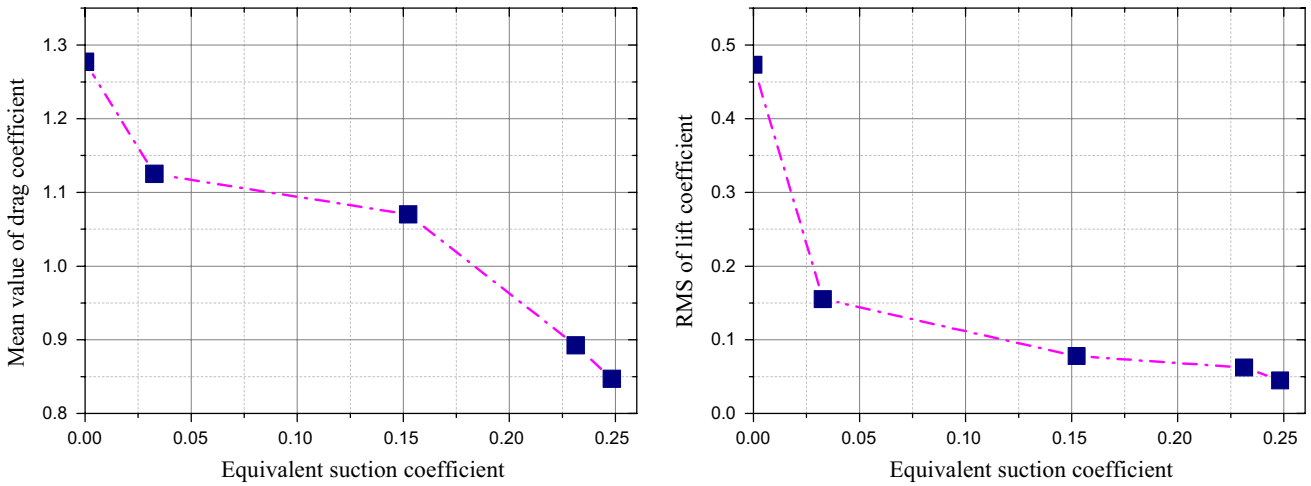

Fig. 9 Lift and drag coefficients of the test model with and without passive jet control

different test cases (including the baseline case and the four controlled cases) can be calculated, and the results are shown in Fig. 9, which can be used to evaluate the effectiveness of the passive jet control technique more quantitatively. It can be seen clearly that the implementation of the passive jets control technique can greatly reduce the drag and lift acting on the cylindrical test model. When the equivalent suction coefficient C_{suc} equals 0.037, i.e., for the test case N1, while the mean drag coefficient obtains a reduction by 11.9 %, the RMS value of the lift coefficient witnesses a remarkable drop by 67.2 %, in comparison with the baseline case. With the C_{suc} increases, both mean drag and RMS value of the lift coefficients experience a downward trend. As C_{suc} grows to 0.1524 (i.e., the test case N5), 16.2 % of drag reduction and 83.5 % suppression of lift RMS value are obtained. When C_{suc} reaches 0.2313 (i.e., the test case N9), the drag coefficient is reduced up to 30.1 % and the RMS value of the lift coefficient is suppressed up to 86.8 %. After a slight increase in C_{suc} (0.2483), the test case N13 experiences a marginal but consistent reduction in both the mean drag (33.7 %) and the RMS value of the lift (90.6 %). Reasonably, the passive jet control technique reaches its peak effect at the maximum C_{suc}. It should be noted that when the value of

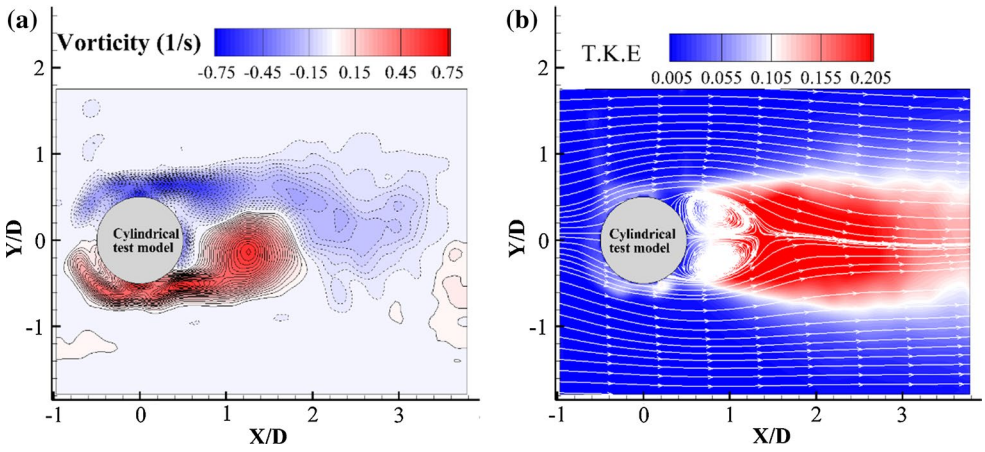

Fig. 10 PIV measurement results in wake behind the test model for the baseline case without passive jet control. **a** Instantaneous flow field. **b** Time-averaged flow field

C_{suc} is 0.1524, the RMS value of the lift coefficient drops below 0.1, which demonstrates the fluctuating lift could be significantly suppressed even for the test case N5.

3.2 PIV measurement results

As described above, a high-resolution PIV system was employed in the present study to quantify the flow characteristics of the wake behind the cylindrical test model in order to gain a further insight into the mechanism of the passive jet control technique. In the present study, snapshot proper orthogonal decomposition ('snapshot POD') introduced by Sirovich (1987) is adopted for the post processing of the PIV measurement results. The first five POD modes are used to reconstruct the flow structures, as suggested in Meyer et al. (2007). Quoting the finding of Meyer et al. (2007), 'If a flow has dominant flow structures, these are therefore reflected in the first POD modes and hence a given snapshot can often be reconstructed satisfactorily using only the first few modes'.

Figure 10 shows the PIV measurement results (both instantaneous and time-averaged flow fields) of the wake flow behind the cylindrical test model for the baseline case without passive jet control. As shown in the instantaneous PIV measurement, a pair of antisymmetric vortex structures is shed from each side of the cylinder, and a Karman vortex street is observed to form in the wake behind the cylinder. The alternative shedding of the unsteady wake vortex structures from sides of the cylinder would cause dramatic variations of the surface pressures around the cylinder, especially in the flow separation region on the leeward side of the test model, as shown from the surface pressure measurement results given in Fig. 5. As a result, the wind loads acting on the cylinder, both lift and drag forces, would be fluctuating dramatically, which could excite vortex-induced vibration if the cylinder was not rigidly mounted. The time-averaged PIV measurement result of the baseline case given in Fig. 10b reveals that flow separations are found near the azimuthal angles of 90° and 270°. As shown in Fig. 5, the plateau region in the surface pressure profile starts at 90° and ends at 270° and indicates the locations of two separation points for the baseline case, which is in good agreement with the flow topology revealed from the PIV measurements. Owing to the flow separation, a large recirculation region is observed to form in the wake behind the cylinder and cause pressure difference between the windward and leeward sides of the cylinder. In addition, the turbulent kinetic energy (TKE) values in the wake are found to be quite high, especially along the shedding paths of the vortex structures. Note the TKE values, which are associated to the vortex structures, are usually used as the measurement of the turbulence mixing in the wake flow (Benard et al. 2008). Moreover, TKE values in the wake flow can also be used to indicate the unsteadiness of the surface pressures and the fluctuating amplitude of the resultant dynamic wind loads acting on the cylinder (Chen et al. 2014). Therefore, TKE values in the wake flow behind the test model are adopted as an indicator to assess the effectiveness of the passive jet control in the present study.

Typical instantaneous vortex structures in wake flow behind the cylindrical test model for the controlled cases obtained by PIV measurements are given in Fig. 11. As expected, a pair of symmetric jet vortices is found to form in the near wake behind the cylindrical test model for the test case N1. The jet flows into the wake and modifies the pattern of wake vortex shedding by interacting with the wake vortices behind the cylindrical test model. As a result, the region of the vortex formation is elongated and pushed further downstream. Despite the modifications in the near wake, the alternating vortex shedding from the cylinder is still observable, which explains the existence of dominant frequency in the power spectrum of the measured lift force for the test case N1 as shown in Fig. 8. For the test case N5, the jet vortex pair is also noticeable, and the process of the elongation and modification is further enhanced. With

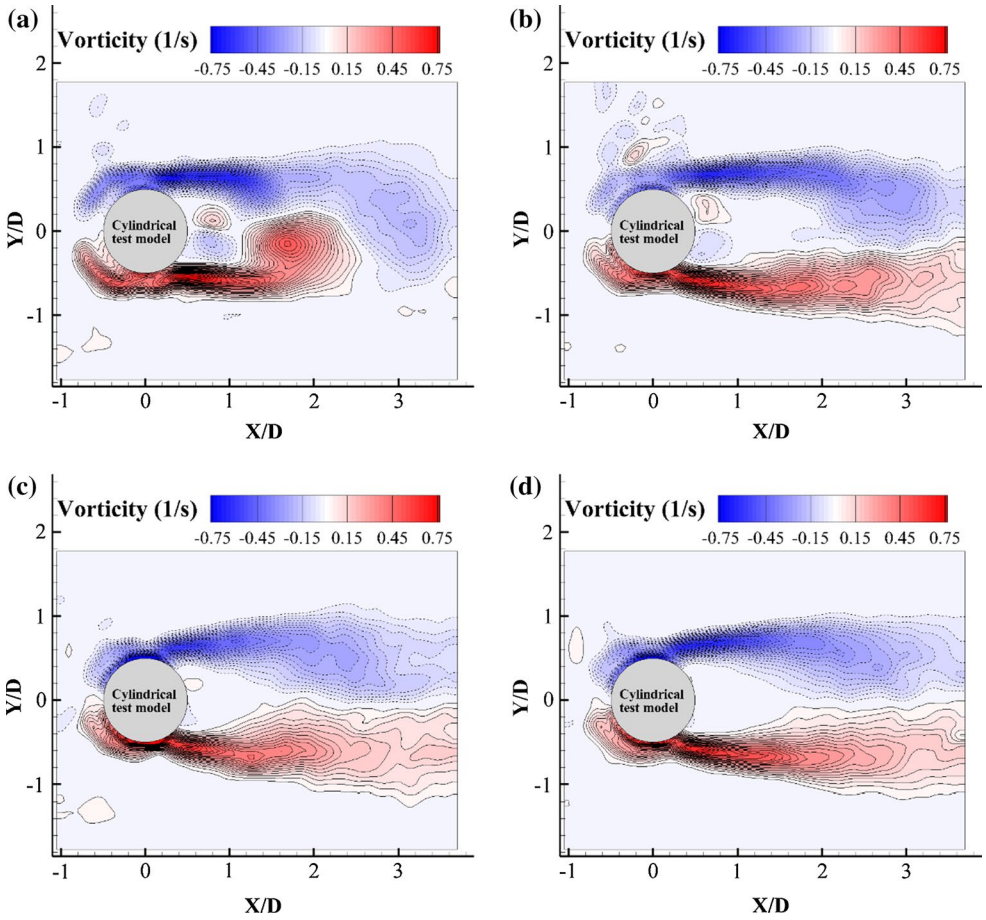

Fig. 11 The instantaneous PIV measurement results in wake behind the test model for the controlled cases. **a** Case N1. **b** Case N5. **c** Case N9. **d** Case N13

the two arrays of vortices tend to detach, the antisymmetric pattern of the vortex shedding is roughly changed to symmetric in the wake behind the cylinder, which is in good agreement with the previous result reported in Feng et al. (2010). When the jet flows from the jet holes are not strong enough, i.e., for the test cases N9 and N13, no distinct jet vortex pair is observed in the instantaneous PIV results, but they can still contribute effectively to the elongation of the shear layers and the modification of the wake vortex shedding pattern in the wake flow behind the cylindrical test model. Due to the enhanced jet flow into the wake for the test cases N9 and N13, two arrays of wake vortices with opposite sign are noticeable, indicating the pattern of the wake vortex shedding has been completely converted into a symmetric mode. Correspondingly, the RMS value of the measured instantaneous lift forces acting on the cylinder are substantially decreased, in comparison with that of the baseline case. Liu and Feng (2015) proposed that the suppression of the lift fluctuation on a circular cylinder could be realized by inducing a symmetric vortex shedding mode in the wake. The flow structures and pressure measurement results reported in the present study confirm their conjunctures. Moreover, since the alternating vortex shedding has been eliminated for the test cases N9 and N13, the time periodicities of the resultant aerodynamic forces acting on the test model are fading away. This explains the disappearance of the dominant frequency in the power spectrum of the measured dynamic lift forces acting on the test model, as shown in Fig. 8. While the region of the vortex formation behind the cylinder is pushed further downstream for the test cases N9 and N13, the drag force acting on the test model reaches the minimum, as described above.

Time-averaged flow structures obtained by PIV measurements for the controlled cases are illustrated in Fig. 12. For the test case N1, the flow jets into the near wake through the jet hole and interacts with the recirculating flow in the wake behind the cylinder. As a result, two recirculation regions, an upstream one and a downstream one, are found to form in the wake behind the test model. Though the wake vortices shed from two sides of the cylinder still exist, the jet flow pushes them further downstream, and the recirculation region becomes larger in comparison with that of the baseline case. The upstream recirculation region is not as obvious as that reported by Feng et al. (2010) and Baek and Karniadakis (2009), this is mainly because the vortices jet into the wake is relatively small and the downward velocity

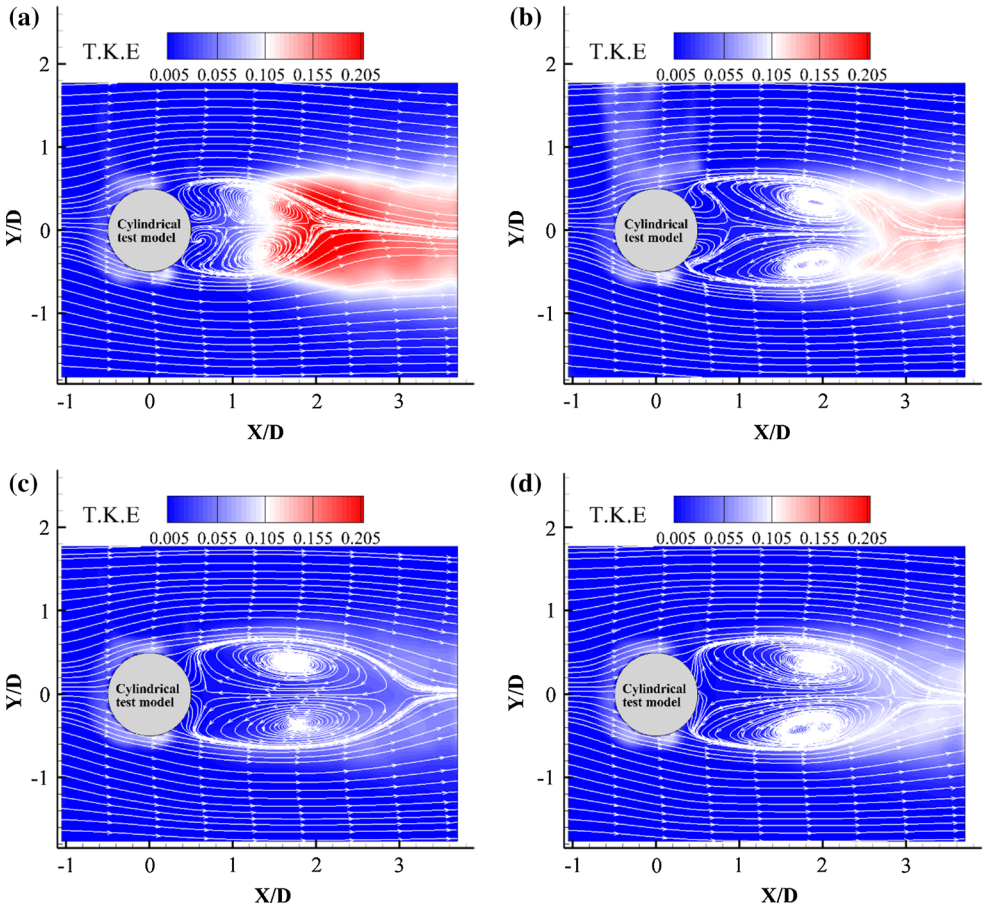

Fig. 12 The time-averaged PIV measurement results in the wake behind the test model for the controlled cases. **a** Case N1. **b** Case N5. **c** Case N9. **d** Case N13

is quickly dissipated in the competition with the strong reversing flow. It is noteworthy that the distribution of TKE in the wake behind the test model has been greatly changed, in comparison with that of the baseline case. Clearly, while the TKE levels in the wake flow were found to become smaller in general, the region with high TKE values is pushed far away from the cylinder, which indicates a lower turbulence level in the near wake behind the test model for the test cases with passive jet control. As a result, the unsteadiness of the surface pressure and the fluctuating amplitude of the resultant dynamic wind loads acting on the test model are suppressed. Moreover, with the increase in the suction holes, the jet process is no longer confined to the region near the rear stagnation point and the jet velocity becomes relatively smaller. Therefore, the recirculation regions in the upstream tend to be pulled back to the side walls of the test model according to the streamline pattern shown in Fig. 12. It can also be seen that the absolute TKE levels in the wake flow become lower in general for the test cases with more suction holes, which indicates a better suppression in fluctuating wind loads acting on the test model for the test cases with more suction holes.

3.3 Linear stability analysis

As revealed clearly from the PIV measurement results given above, the wake flow pattern and wake vortex shedding mode at the two sides the cylinder have been modified significantly after the implementation of passive jet control to the cylindrical test model. It is worth noting that the vortex formation behind a stationary cylinder is usually associated to the absolute instability in the wake, as suggested in Triantafyllou et al. (1986). Since the cylindrical test model used in the present study is set to be stationary during the experiments, it is appropriate to employ linear local stability analysis theory to explore the underlying mechanism of the passive jet control technique, by following the work described in Dong et al. (2008), Baek and Karniadakis (2009).

Figure 13 illustrates the streamwise velocity profiles in the wake behind the cylindrical test model at different downstream location behind the test model, which are extracted from the time-averaged PIV measurement results. While the time-averaged velocity profiles are mostly symmetric about the centerline of the test model in general, some small imperfections can still be seen in the profile due to various minor system measurement errors in the PIV

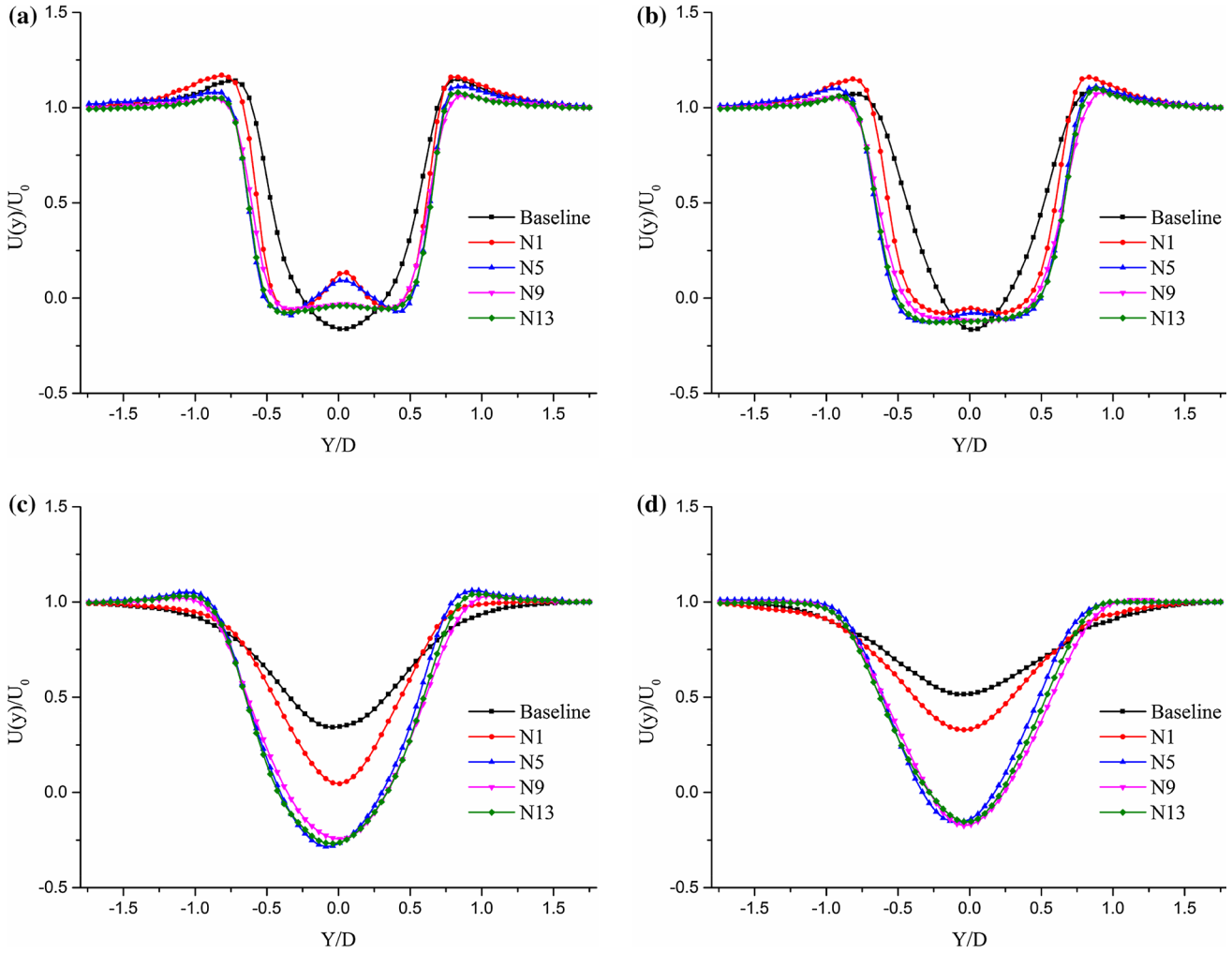

Fig. 13 Time-averaged velocity profiles in the wake flow at the downstream locations of: **a** $X/D = 0.75$. **b** $X/D = 1.0$. **c** $X/D = 2.0$. **d** $X/D = 2.5$

measurements, e.g., the non-perfectly uniform incoming flow, limited frame number of the instantaneous PIV measurements to calculate the time-averaged flow field.

In the very near wake, i.e., at the downstream location of $X/D = 0.75$, local cusps are noticeable in the velocity profiles at $Y/D = 0$ for both the test cases of N1 and N5, which indicates relatively strong jets exhausted from the jet holes. As the passive jets convect downstream, the cusps are found to disappear gradually and are no longer observed after the downstream location of $X/D = 1.0$. In addition, as the downstream distance from the test model increases, the velocity deficits in the profiles gradually recover. It can be seen from Fig. 13 that the velocity deficit in the wake flow behind the test model would recover much slower for the controlled test cases than that of the baseline case, which demonstrates the elongation of the recirculation regions revealed from the PIV measurement results given in Fig. 12. Considering its working mechanism, the transportation capability between the windward and leeward stagnation points plays a crucial role in the passive jet control, and the suction/jet holes arranged near the stagnation points contribute most to the transportation process. As a result, the time-averaged velocity profiles for the test cases N5, N9 and N13 exhibit a similarity after the downstream distance reaches $X/D = 1.0$. On the other hand, since the modification in the wake flow for the test case N1 is not as effective as the other controlled test cases, the recovery of the velocity deficits for the test case N1 is found to be significantly faster than all the other test cases.

Based on the time-averaged velocity profiles extracted from the PIV measurement results at different downstream locations, inviscid Orr–Sommerfeld equation is solved to determine the coordinates of the critical point in the complex frequency plane, as suggested by Triantafyllou et al. (1986). The dispersion relation $\omega = \omega(k)$ maps k_i constant lines on the ω plane at different downstream locations. For different k_i, a bunch of quadratic maps with similar shape can be obtained. The quadratic maps touch at the critical

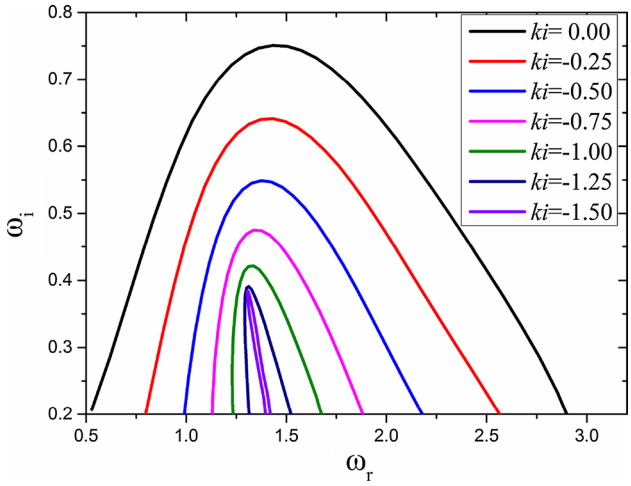

Fig. 14 Map of lines k_i = constant in the ω plane, at $X/D = 0.75$ for the baseline case

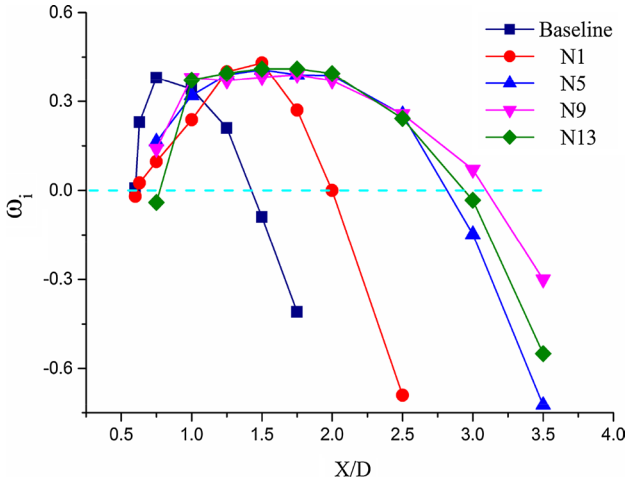

Fig. 15 Imaginary part of the critical point versus X/D for various test cases

point. The nature of the instability is determined by the imaginary part of the complex frequency at the critical point (denoted by ω_i). A positive ω_i suggests absolute instability, which indicates that any initial disturbances will grow at any fixed positions. On the other hand, if ω_i is negative, the instability is then convective, and any initial disturbances will grow with time but is convected away.

Figure 14 gives a map of lines (k_i = constant) in the ω plane, where k is the complex wave number and k_i denotes its imaginary part. This map is derived based on the time-averaged velocity profile behind the test model at downstream location of $X/D = 0.75$ for the uncontrolled case. The mapped curves touch at the critical point, which looks like a cusp on the plane. As revealed from Fig. 14, the imaginary part of the critical point can be clearly observed as 0.38, while its real part (denoted by ω_r) is 1.31. Therefore, the wake flow behind the cylindrical test model at the downstream location of at $X/D = 0.75$ for the uncontrolled case supports an absolute instability, which leads to the formation of a vortex street as observed in the experiments. Furthermore, the corresponding Strouhal number (St) can be derived from the value of ω_r by $St = \omega_r/2\pi = 0.2085$, which is in good agreement with the result obtain by the power spectrum analysis of the measured dynamic lift forces acting on the test model (i.e., $St = fD/U = 0.21$) discussed above.

Figure 15 shows the values of ω_i at different downstream locations for the baseline and 4 controlled cases. It can be seen that, while a region of absolute instability is observed in the wake for the uncontrolled baseline case, the disturbance growth rate ω_i for all the controlled cases is found to decrease in the immediate wake (i.e., the region of $X/D < 1.0$) and the absolute instability zone is shifted further downstream. For the baseline case, the wake is found to be converted into convective instability after the downstream location of $X/D = 1.4$. The linear stability analysis also predicts that the local growth rate ω_i would reach its peak at the downstream location of $X/D = 0.75$, which is close to the center of vortices formed in the wake behind the cylinder for the uncontrolled baseline case, as shown in Fig. 10b. For the test case N1, while the absolute instability zone is displaced downward, the maximum growth rate is found to be larger than that of the baseline case. This is consistent with the findings reported in the previous study of Baek and Karniadakis (2009). In addition, the peak growth for the test case N1 is found to occur in the neighborhood of $X/D = 1.5$. As revealed from the time-averaged flow field given in Fig. 12, the recirculation region for the test case N1 is elongated and pushed further downstream due to the passive jet flow exhausted from the jet hole at the rear stagnation point of the test model. As a result, the centers of jet vortices are shifted downward to the location of $X/D \approx 1.4$, which agrees reasonably well with finding of the linear stability analysis. Figure 15 also reveals that, as the number of the suction/jet holes increases, the absolute instability region would to shift further downstream. As shown clearly in Fig. 13, the velocity profiles for the test cases N5, N9 and N13 would exhibit good similarity in the downstream locations between $X/D = 1.0$–2.5. Since the velocity profiles of the time-averaged flow is the base for the linear stability analysis, the disturbance growth rate of these test cases are expected to be quite close to each other within such downstream locations. This is confirmed by the results of the stability analysis, as shown in Fig. 15. For the test cases N5, N9 and N13, the predicted maximum growth rates occur in range of the downstream locations of $X/D = 1.5$–2.0. Accordingly, the centers of the wake vortices are found to appear in the neighborhood of

the downstream location of $X/D \approx 1.8$, as shown in Fig. 12. Interestingly, it is the test case N9, instead of the test case N13, whose absolute instability pump is found to be expanded broadest along the streamwise direction. This is mainly because that the velocity of the jet flows exhausted from the jet holes for the test case N9 is marginally larger than that of the test case N13, which can modify the wake flow in a farther region.

4 Conclusions and discussions

In the present study, an experimental campaign was conducted to investigate the effectiveness of a passive jet flow control scheme to manipulate the vortex shedding process from a circular cylinder in order to reduce the fluctuating amplitudes of the dynamic wind loads acting on the cylinder. The passive flow control scheme, characterized by passive windward suction combined with leeward jet, was realized by using perforated pipes to create flow communicating channels between the windward and leeward stagnation points of a cylindrical test model. The experimental study was performed in a wind tunnel at a Reynolds number of $Re = 4.16 \times 10^4$ based on the cylinder diameter and oncoming flow speed. In addition to the surface pressure measurements, a digital particle image velocimetry (PIV) system was also used to achieve detailed flow field measurements to quantify the flow characteristics of the wake flow behind the cylindrical model for the test cases with and without passive jet flow control.

The measurement results reveals that, while the fluctuation amplitudes of the instantaneous lift forces acting on the cylinder could be significantly suppressed due to the passive jet control, the mean drag force coefficients of the test model were also found to become much smaller for the controlled cases, in comparison with the baseline case. In addition, a higher equivalent suction coefficient C_{suc} was found to contribute to a better flow control effectiveness by using the passive jet control scheme. The quantitative PIV flow field measurements confirmed the findings derived from the surface pressure measurements. In comparison with those of the baseline case without flow control, recirculation regions behind the test model for the test cases with passive jet flow control were found to be elongated and pushed further downstream owing to the interaction of the jet flows exhausted from the jet holes near the rear stagnation point of the test model with the wake flow. Moreover, the TKE levels in the wake flow behind the test model were also found to be much smaller for the test cases with passive jet control, in comparison with that of the baseline case. Apart from the power spectrum analysis of the dynamic wind loads acting on the test model, the instantaneous wake vortex structures revealed from the PIV measurement results also confirmed that the passive jet flow control method could manipulate the shedding process of the wake vortices from two sides of the cylindrical test model effectively. Linear stability analysis suggested that the jets exhausted from the holes on leeward surface of cylindrical model would modify the wake stability behind the cylinder by displacing the region of absolute instability further downstream. Linear stability analysis also demonstrated the similarity of the wake flow pattern for the test cases with sufficient suction/jet holes to realize the passive jet control scheme. Since the mechanism of the passive jet control scheme is to form a communicating channel between the windward and leeward stagnation points, the transportation capability of flow between windward and leeward stagnation points has been found to decide the flow control effectiveness.

The passive jet control technique described here is relatively easy to implement for various engineering applications, even for the existing stay-cabled bridges. While the perforated pipe design with 5 pair of suction/jet holes (i.e., the test case N5 of the present study) were found to be able to substantially suppress the fluctuating amplitude of the dynamic wind loads acting on the circular cylinder, the perforated pipe design with evenly distributed suction/jet holes around the circular cylinder (i.e., the test case N13) is highly recommended for engineering applications since the angle of attack of the incoming wind may vary significantly in the field.

It should also be noted that although the effectiveness of the passive jet control scheme has been proved based on the pressure measurements and the detailed flow field measurement result reported in the present study, some important questions remains unsolved. For example, as described in Owen and Bearman (2001), flow control techniques often confront a fundamental limitation. They may exhibit distinctive effectiveness for dynamic wind loading suppression for fixed cylinders, while they will not work well for elastically mounted structures. It is also well known that the flow characteristics behind a circular cylinder may change significantly as the spanwise length of the cylinder increases, and there may exist a critical spanwise length for the perforated pipe unit beyond which the effectiveness of the passive jet control scheme may be limited. Therefore, further comprehensive studies are still needed to explore/optimize design paradigms to maximize the effectiveness of the passive jet control scheme. As a follow-up of the work presented here, we are planning to conduct an experimental study by employing an elastically mounted cylindrical test model to evaluate the effectiveness of the passive jet control scheme under more realistic conditions for cable-stayed bridge applications. While the effects of the spanwise length of perforated pipe units on the flow control effectiveness will be investigated systematically,

the spanwise variations of the wake flow characteristics behind the circular cylinders with and without passive jet flow control will also be examined in great details by conducting detailed PIV measurements in different spanwise cross-planes. The experimental results will be reported in the near future.

Acknowledgments The authors would like to extend their sincere gratitude to Professor George Karniadakis of Brown University and Professor Dejun Sun of University of Science and Technology of China (USTC) for their thought-provoking discussions on linear stability analysis. This research work is funded by the National Natural Science Foundation of China (NSFC) through Grant 51378153, 51578188, 51008093, 51161120359 and 91215302; and is supported by the Opening Funds of State Key Laboratory of Building Safety and Built Environment.

References

Amitay M, Honohan A, Trautman M, Glezer A (1997) Modification of the aerodynamic characteristics of bluff bodies using fluidic actuators. AIAA paper, 97-2004

Amitay M, Smith BL, Glezer A (1998) Aerodynamic flow control using synthetic jet technology. AIAA paper, 98-0208

Baek H, Karniadakis G (2009) Suppressing vortex-induced vibrations via passive means. J Fluids Struct 25(5):848–866

Barlow B, Rae H, Pope A (1999) Low-speed wind tunnel testing, 3rd edn. Wiley, New York, pp 330–375

Benard N, Balcon N, Touchard G, Moreau E (2008) Control of diffuser jet flow: turbulent kinetic energy and jet spreading enhancements assisted by a non-thermal plasma discharge. Exp Fluids 45:333–355

Brika D, Laneville A (1993) Vortex-induced vibrations of a long flexible circular cylinder. J Fluid Mech 250:481–508

Chen WL, Xin DB, Xu F, Li H, Ou JP, Hu H (2013) Suppression of vortex-induced vibration of a circular cylinder using suction-based flow control. J Fluids Struct 42:25–39

Chen WL, Li H, Hu H (2014) An experimental study on a suction flow control method to reduce the unsteadiness of the wind loads acting on a circular cylinder. Exp Fluids 55(4):1–20

Crook A, Sadri AM, Wood NJ (1999) The development and implementation of synthetic jets for the control of separated flow. AIAA paper, 99-3176

Dong S, Triantafyllou GS, Karniadakis GE (2008) Elimination of vortex streets in bluff-body flows. Phys Rev Lett 100(20):204501

Feng LH, Wang JJ (2010) Circular cylinder wake vortex synchronization control with synthetic jet positioned at back stagnation point. J Fluid Mech 662:232–259

Feng LH, Wang JJ (2012) Synthetic jet control of separation in the flow over a circular cylinder. Exp Fluids 53:467–480

Feng LH, Wang JJ, Pan C (2010) Effect of novel synthetic jet on wake vortex shedding modes of a circular cylinder. J Fluids Struct 26:900–917

Feng LH, Wang JJ, Pan C (2011) Proper orthogonal decomposition analysis of vortex dynamics of a circular cylinder under synthetic jet control. Phys Fluids 23:014106–1–014106–13

Fransson JHM, Konieczny P, Alfredsson PH (2004) Flow around a porous cylinder subject to continuous suction or blowing. J Fluids Struct 19:1031–1048

Fujisawa N, Takeda G (2003) Flow control around a circular cylinder by internal acoustic excitation. J Fluids Struct 17:903–913

Fujisawa N, Takeda G, Ike N (2004) Phase-averaged characteristics of flow around a circular cylinder under acoustic excitation control. J Fluids Struct 19:159–170

Glezer A, Amitay M, Honohan AM (2003) Aspects of low- and high-frequency aerodynamic flow control. AIAA paper, 2003-0533

Hikami Y, Shiraishi N (1988) Rain-wind induced vibrations of cables in cable stayed bridges. J Wind Eng Ind Aerodyn 29:409–418

Irwin H, Cooper R, Girard R (1979) Correction of distortion effects caused by tubing systems in measurements of fluctuating pressures. J Wind Eng Ind Aerodyn 5(1):93–107

Kondo N (1993) Direct third-order upwind finite element simulation of high Reynolds number flows around a circular cylinder. J Wind Eng Ind Aerodyn 46:349–356

Liu YG, Feng LH (2015) Suppression of lift fluctuations on a circular cylinder by inducing the symmetric vortex shedding mode. J Fluids Struct 54:743–759

Meyer KE, Pedersen JM, Özcan O (2007) A turbulent jet in crossflow analysed with proper orthogonal decomposition. J Fluid Mech 583:199–227

Owen JC, Bearman PW (2001) Passive control of VIV with drag reduction. J Fluids Struct 15:597–605

Sirovich L (1987) Turbulence and the dynamics of coherent structures. Part I: Coherent structures. Q Appl Math 45(3):561–571

Triantafyllou G, Triantafyllou M, Chryssostomidis C (1986) On the formation of vortex streets behind stationary cylinders. J Fluid Mech 170:461–477

Wolfe D, Ziada S (2003) Feedback control of vortex shedding from two tandem cylinders. J Fluids Struct 17:579–592

Zdravkovich MM (1981) Review and classification of various aerodynamic and hydrodynamic means for suppressing vortex shedding. J Wind Eng Ind Aerodyn 7(2):145–189

Zuo D, Jones NP (2010) Interpretation of field observations of wind- and rain-wind-induced stay cable vibrations. J Wind Eng Ind Aerodyn 98:73–87

Zuo D, Jones NP, Main JA (2008) Field observation of vortex- and rain-wind-induced stay-cable vibrations in a three-dimensional environment. J Wind Eng Ind Aerodyn 96:1124–1133